CardiacWave: A mmWave-based Scheme of Non-Contact and High-Definition Heart Activity Computing

CHENHAN XU and HUINING LI, University at Buffalo, USA
ZHENGXIONG LI, University at Buffalo, USA and University of Colorado Denver, USA
HANBIN ZHANG, ADITYA SINGH RATHORE, and XINGYU CHEN, University at Buffalo, USA
KUN WANG, University of California, Los Angeles, USA
MING-CHUN HUANG, Duke Kunshan University, China
WENYAO XU, University at Buffalo, USA

Using wireless signals to monitor human vital signs, especially heartbeat information, has been intensively studied in the past decade. This non-contact sensing modality can drive various applications from cardiac health, sleep, and emotion management. Under the circumstance of the COVID-19 pandemic, non-contact heart monitoring receives increasingly market demands. However, existing wireless heart monitoring schemes can only detect limited heart activities, such as heart rate, fiducial points, and Seismocardiography (SCG)-like information. In this paper, we present CardiacWave to enable a non-contact high-definition heart monitoring. CardiacWave can provide a full spectrum of Electrocardiogram (ECG)-like heart activities, including the details of P-wave, T-wave, and QRS complex. Specifically, CardiacWave is built upon the Cardiac-mmWave scattering effect (CaSE), which is a variable frequency response of the cardiac electromagnetic field under the mmWave interrogation. The CardiacWave design consists of a noise-resistant sensing scheme to interrogate CaSE and a cardiac activity profiling module for extracting cardiac electrical activities from the interrogation response. Our experiments show that the CardiacWave-induced ECG measures have a high positive correlation with the heart activity ground truth (*i.e.*, measurements from a medical-grade instrument). The timing difference of P-waves, T-waves, and QRS complex is 0.67%, 0.71%, and 0.49%, respectively, and a mean cardiac event difference is within a delay of 5.3 milliseconds. These results indicate that CaridacWave offers high-fidelity and integral heart clinical characteristics. Furthermore, we evaluate the CardiacWave system with participants under various conditions, including heart and breath rates, ages, and heart habits (*e.g.*, tobacco use).

CCS Concepts: • **Computer systems organization** → **Embedded and cyber-physical systems**; • **Human-centered computing** → **Ubiquitous and mobile computing systems and tools**; • **Applied computing** → *Health care information systems*.

Additional Key Words and Phrases: Millimeter Wave Sensing

Address comments to wenyaoxu@buffalo.edu.
Authors' address: Chenhan Xu; Huining Li; Zhengxiong Li; Hanbin Zhang; Aditya Singh Rathore; Xingyu Chen; Wenyao Xu, University at Buffalo, the State University of New York, Department of Computer Science and Engineering, Amherst, NY, 14260, USA. Kun Wang, University of California, Los Angeles, Electrical and Computer Engineering Department, Los Angeles, CA 90095-1594, USA. Ming-chun Huang, Duke Kunshan University, Kunshan, Suzhou, Jiangsu, 215316, China.

1 INTRODUCTION

Electronic tools for cardiac activity monitoring, including Electrocardiogram (ECG), are an important clinical approach that tracks and diagnoses the health status of human hearts. The market of cardiac monitoring tools is expected to reach $6,637 million by 2023 [65]. However, current practice in cardiac monitoring still mainly employs contact skin-irritating attachments (*i.e.*, electrodes and sensors) that could result in unpleasant user experience and medical waste.

In recent decades, non-contact cardiac monitoring solutions have been widely explored. The mainstream of non-contact cardiac monitoring is based on the thorax wall vibration from cardiac beat activities. This vibration can be detected through Doppler effects [46] using wireless wave-signals. For example, systems using WiFi signals [69] and RFID technologies [78] are investigated to measure chestwall coarse vibrations and then estimate the basic heart parameters, such as heart rate. Recent studies leverage higher-frequency sensing modalities, *e.g.*, mmWave [26] and laser sensors [43], to achieve the recording of thorax vibrations. However, the underlying mechanism of these works rely on Doppler effects, which can only manifest limited cardiac activities (*e.g.*, heart rate and SCG-like signals) due to the inconsistency of measuring locations and signal-to-activity correspondence among literature [63].
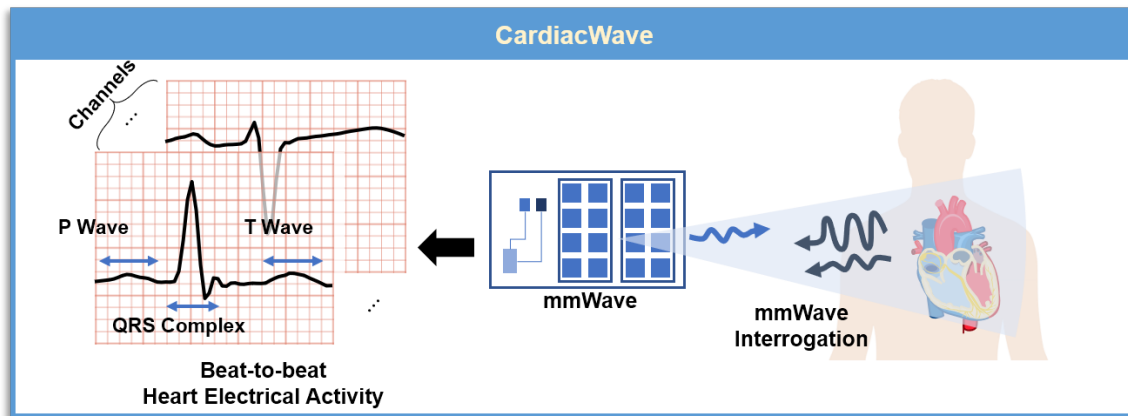

Fig. 1. CardiacWave is a non-contact sensing solution to monitor high-definition heart activities via mmWave scattering on chest.

To date, the golden tool to clinically characterize cardiac activities is still the ECG devices. The correspondence between ECG and several major cardiac physiological events is described as a fiducial point system [35]. For example, the ECG P wave is related to atrial depolarization, QRS complex, and T wave correspond to the ventricular depolarization and repolarization, respectively. Being aware of the advantages of ECG, previous study [11] proposed to use the photoplethysmography that can be acquired from remote face camera [34] to estimate the ECG parameters. However, camera is sensitive to the ambient light and the proposed method still lacks granularity, *i.e.*, the ECG signal is not sensed. As a result, a fine-granularity and non-contact cardiac electrical activity monitoring system is still an open challenge.

In this paper, we present CardiacWave, a remote and high-granularity heart monitoring system, as shown in Figure 1. CardiacWave brings two significant advantages to cardiac electrical activity computing: **(1) Unobtrusive**: CardiacWave performs remote and device-free cardiac electrical activity monitoring. Therefore, users can get rid of cumbersome electrodes and the skin condition such as sweat will not influence the monitoring quality.

(2) Informative: CardiacWave can monitor the cardiac electrical activity from *multiple axes (i.e., channels)* and provide ECG-like high-resolution, multi-channel measures.

CardiacWave is based on the Cardiac-mmWave scattering effect (CaSE) that the electromagnetic (EM) field induced by cardiac electrical activity will modulate the chest-scattered mmWave signals with activity information. Though the CaSE guides us a promising path, constructing CardiacWave is still non-trivial because the cardiac EM field is a complex field sourced from numerous cardiac cells. Moreover, the field varies with time due to the periodical cardiac activity. Acknowledging this, we remark three challenges to be addressed to realize CardiacWave. **(a) Remote and integral sensing of CaSE**. In order to get the CaSE response, we leverage the frequency modulated mmWave with 4-GHz bandwidth for integral interrogation. Then, the interrogation response is demodulated combining time and frequency domain information and the noise is eliminated. Afterwards, we employ mask-based learnable filters to extract integral CaSE features. **(b) Cardiac activity profiling for ECG signals generation**. Reconstructing ECG-like signals from the extracted CaSE features is challenging due to the complex coupling between CaSE and ECG signals. We first analyze the bridging mechanism, *i.e.*, the ionic concentration in cardiac cells is the root of cardiac EM field and ECG signals. Knowing the mechanism, we model the signal reconstruction as solving a partial differential equation problem. We develop a data-driven deep neural network that can profile the cardiac activity as a solver, thereby reconstructing multi-channel and high-resolution ECG-like signals. **(c) Comprehensive evaluation of CardiacWave**. Aiming for unobtrusive and informative heart electrical monitoring, we design and conduct experiments from *cardiac event integrity* and *signal fidelity* perspectives. Experiment results show that the normalized error of P waves, T waves, QRS complex, R-R interval, Q-T interval are less than 0.91%. The correlation coefficients between the reconstructed ECG-like signal and ECG baseline is around 0.9. Further usability and robustness analyses show that CardiacWave's performance will not be impacted by the body conditions and wearable accessories.

To conclude, our contribution has the following three aspects:

• We propose a new non-contact and high-definition scheme of cardiac electrical activity computing by exploring the cardiac-mmWave scattering effect (CaSE). We discover that the cardiac electromagnetic field modulates rich cardiac electrical activity information into the chest-scattered mmWave response.

• We develop CardiacWave to provide ECG-like high-resolution and multi-channel measures. CardiacWave utilizes frequency-modulated mmWave to interrogate the CaSE. A deep neural network-based cardiac activity profiler is designed for reconstructing full ECG-like signal from CaSE features.

• We conduct extensive experiments over 40 subjects. We demonstrate that generated ECG-like signals have high integral cardiac events and signal fidelity. Moreover, CardiacWave is robust to the muscle excitation during the daily activity, where ECG signals are not appliable.

2 RELATED WORK

Non-contact heart monitoring has attracted much attention in the recent ten years. Different from the traditional approaches (*e.g.*, attaching sensors on chest [14], neck [38], wrist [9], arm [76], and foot [41]), non-contact heart monitoring enables sensor-free solutions where user experience will not be degraded because of skin irritation or activity limitation.

Existing non-contact cardiac monitoring is mainly based on the thorax wall vibration caused by cardiac activity. In the early stage, many works leverage WiFi and RFID to detect heart rate viability and fiducial points [69, 72]. Zhao et al. [77] used RF signals to extract individual heartbeats for emotion recognition. Lin et al. [46] employed 2.4 GHz Doppler radar to implement a non-contact and continuous sensing system to capture heart rate and fiducial points for user authentication. Zhao et al.[78] developed an RFID-based non-contact respiration and heartbeat monitoring system. With the promotion of sensing technology, recent works start to explore Seismocardiography (SCG)-like information. Kroschel et al. [43] proposed a laser-based remote measurement approach for achieving

SCG-like vital parameters. Ha et al. [26] leveraged a 77 GHz FMCW radar and deep learning technology to develop an RF-SCG system that can capture SCG-like signals without contacting the human body. In addition, camera is used for capturing the Photoplethysmogram (PPG)-like and Ballistocardiogram (BCG)-like information [36, 64]. However, these existing non-contact cardiac monitoring works limit the potential in healthcare and medical applications because they only monitor the heart from a single axis (channel) and are not able to provide high-resolution cardiac activity information.

Different from the existing systems, CardiacWave is the first non-contact system designed to provide multi-channel and high-definition Electrocardiogram (ECG)-like heart activities, including P waves, T waves, and QRS complex, which are the de facto analytical framework of heart-related inspection and research. To achieve the goal, CardiacWave utilize the cardiac-mmWave scattering effect to interrogate the cardiac electrical activity. We introduce the rationale behind CardiacWave next.

3 BACKGROUND AND PRELIMINARIES

3.1 Cardiac-mmWave Scattering

Heart is the principal organ in human circulatory system that pumps blood to deliver nutrients and oxygen to body parts. To pump blood, heart contracts rhythmically, which is driven by the coordinated polarization of an enormous number of cardiac cells (*i.e.*, cardiac electrical activity) [25]. The cardiac cells can generate current via polarization and depolarization, acting as source elements that produce a significant varying electromagnetic (EM) field [66]. As illustrated in Figure 2, heart and its EM field can be modeled as a electric dipole system [40]. Clinical ECG system measures the current on the body surface to solve the current density of the source elements [48], thereby helping cardiac disease diagnosis. Considering the magnetic part of the cardiac EM field can extend outside the body, polarized high-frequency EM waves, *i.e.*, mmWave, can be rotated during the scattering over the chest surface due to the Faraday effect [74]. The scattered mmWave therefore is modulated and carries the varying cardiac EM field information in its frequency, namely Cardiac-mmWave Scattering effect (CaSE). **Hypothesis:** As the electric field is associated with the magnetic field by Maxwell's equation [67], as depicted in the Figure 2, we hypothesize that it is possible to leverage the CaSE for cardiac electrical activity information interrogation, which contributes towards ECG signal reconstruction.
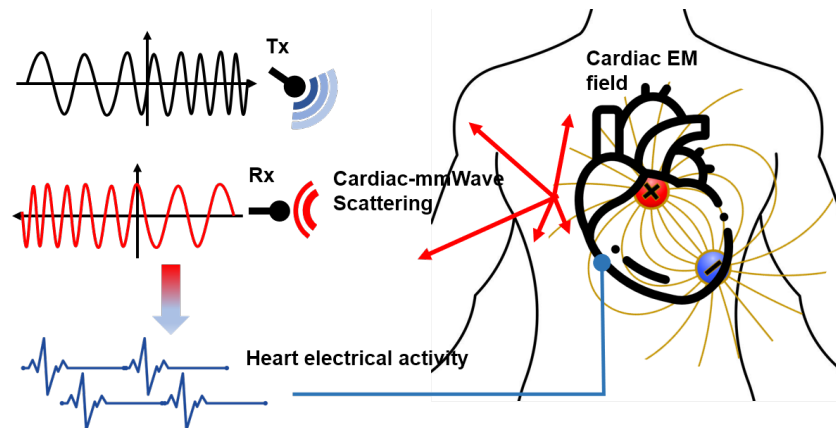

Fig. 2. Cardiac electric activity that ECG measure can be sensed by mmWave via Cardiac-mmWave scattering effect.

3.2 Proof-of-concept Study

To support the hypothesis, we design and conduct preliminary experiments in a controlled environment.

3.2.1 Setup and protocol. During the experiments, a subject wears a portable cardiac monitor Shimmer [58] (see Section 7.2 for sensor specifications). The subject is first asked to do squats to increase the cardiac activity intensity. Then, the subject sits in front of a 76-GHz mmWave probe, aligning chest center to the mmWave probe. We choose Frequency-Modulated Continuous Wave (FMCW) as the emitting waveform for an easy separation of the chest movement's influence, including breathing and heartbeat impacts, in further analysis. The probe continuously emits mmWave and receives the response. Simultaneously, the cardiac monitor records the corresponding cardiac electrical activity for reference. The subject is asked to hold their breath for five cardiac cycles as their heart rate gradually falls back to the resting level (*i.e.*, from 120 BPM to 70 BPM). Since the breathing impact is mitigated, we proceed with the corresponding mmWave responses.

3.2.2 Analysis and summary. We analyze the mmWave response via FMCW intermediate frequency (IF), which is the subtraction between the emitted signal and the mmWave response in the frequency domain (*i.e.*, mixing). In this way, we can further isolate the impact of chest movement induced by heartbeat while retaining the varying CaSE information. Figure 3 shows the IF of two distinct cardiac electrical activities, *i.e.*, atrial depolarization and ventricular repolarization, and their difference with different heart rates (70 BPM versus 120 BPM). The IF is averaged over five cardiac cycles to suppress random noise and the frequency bands containing clutters from chest movement are labeled. We observe that the responses on CaSE bands are *nonidentical* for distinct types of cardiac electrical activity over the frequency spectrum. Moreover, the mmWave responses are *different* when the activity intensity changes. As the mmWave response varies based on the types and the intensity of the cardiac electrical activity, our hypothesis is validated.

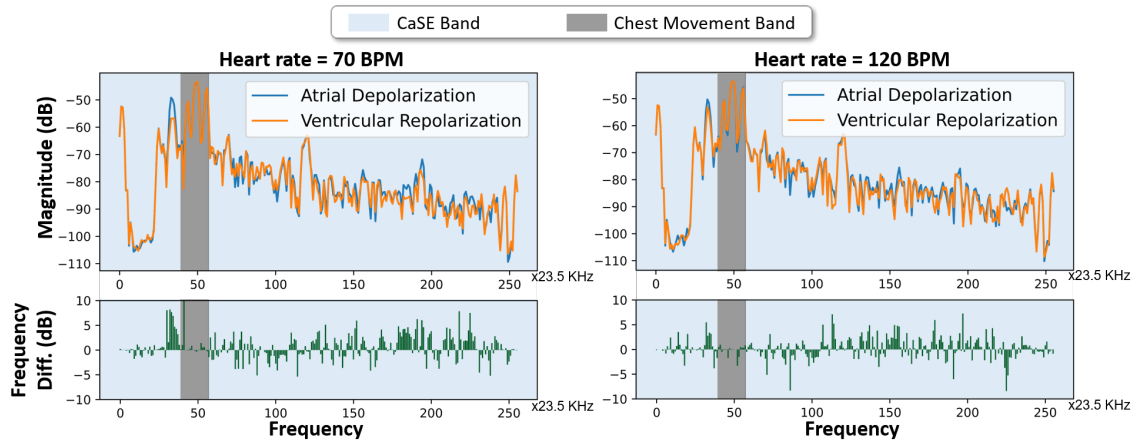Fig. 3. The cardiac-mmWave scattering responses of different cardiac activity types and the frequency differences. The blue area indicates the frequency bands of CaSE and the dark area contains potential clutter from chest movement. (Left: heart rate = 70 BPM; Right: heart rate = 120 BPM).

3.3 Design Targets

Having explored the relation between ECG and CaSE, we have the following two design targets for CardiacWave:

- **CaSE integral sensing**. The cardiac EM field exists around the human chest and varies over time. To acquire the integral information of the EM field, an integral CaSE sensing is demanded.
- **Multi-channel ECG generation**. ECG signals contain rich information about heart electrical activities including but not limited to the cardiac events, which are distributed in multiple channels. Therefore, CardiacWave aims to reconstruct multi-channel ECG-like signals from the sensed CaSE response, thereby boosting heart electrical activity computing.

4 CARDIACWAVE OVERVIEW

In this paper, we present CardiacWave, a first non-contact multi-dimension cardiac electrical monitoring solution. CardiacWave is designed to have an *akin architecture to the existing sensors that have physical quantity sensing and convert-to-signal modules (e.g., microphone).* The two modules that form CardiacWave's sensor-like architecture are illustrated in Figure 4.
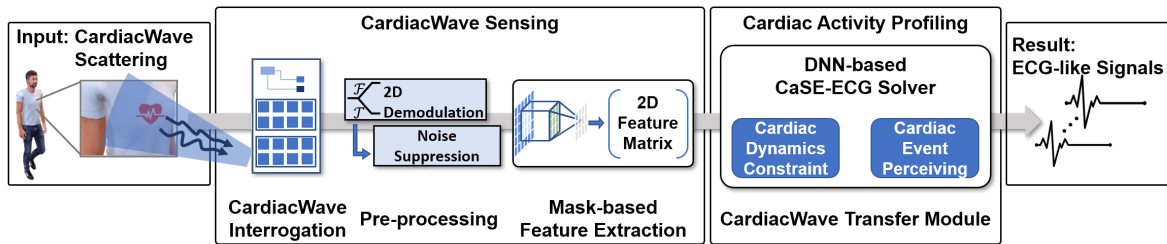

Fig. 4. The overview of CardiacWave. CardiacWave leverages mmWave to interrogate cardiac EM field. The scattered mmWave response is fed to feature extraction and cardiac activity profiling module to reconstruct multi-channel ECG-like signal.

- **CardiacWave Sensing**. CardiacWave sensing scheme is designed to capture the integral CaSE response. In terms of functionality, this front-end module is analog to the diaphragm that senses air vibration in the MEMS microphone. We first interrogate the CaSE via 76 GHz frequency-modulated mmWave with superior sensing capacity. Since the CaSE response varies over time, we demodulate the response in both time and frequency domains. The noise in the generated response matrix is then suppressed to increase the signal-to-noise ratio. Afterward, we develop learnable masks to extract the integral CaSE features from the response matrix.
- **Cardiac Activity Profiling**. Cardiac activity profiling is to generate ECG-like signals from the interrogated CaSE features. This software-based module is analog to the coil in the MEMS microphone that converts the vibration to the digital signal in terms of functionality. By analyzing the common root of cardiac EM field and ECG signals, we deduce the CaSE-ECG coupling as a partial differential equation. A deep neural network (DNN) based cardiac activity profiler is developed to solve the equation. In particular, the profiler utilize recurrent architecture to capture the cardiac dynamics constraint. Then, a wavelet-based error function is applied to perceive the cardiac event during the DNN optimization.

5 CARDIACWAVE SENSING SCHEME

In this section, we elaborate on the sensing scheme by first modeling the CaSE. Then, a mmWave-based interrogation and pre-processing are detailed, followed by a mask-based CaSE feature extraction.

5.1 CardiacWave Modeling

The CaSE, as illustrated in the Figure 2, is related to the frequency shift of mmWave response due to the cardiac activity-induced variable EM field. Specifically, the variable cardiac magnetic field H is distributed about the location and time [39], which can be described as:

$$4\pi H(t,r) = \int_V \hat{J(t)} \times \nabla(\frac{1}{r})\,dv, \tag{1}$$

where r is the distance from an external field point at which H is evaluated to an element of volume dv inside the body, $\hat{J(t)}\,dv$ is a source element of cardiac EM field with current density $\hat{J(t)}$, and ∇ is an three-dimensional gradient operator. Consequently, the mmWave scattering on chest will be impacted by a path-dependent mismatch factor $\beta_L(t)$ [37] because of the magnetic field influence on the polarization of the mmWave [70], expressed as:

$$\beta_L(t) = \int_L \cos^2(\mathcal{V}\mu H(t,r)\,dl), \tag{2}$$

where $\mathcal{V}$ is Verdet constant [17], μ is the permeability, and L is the mmWave propagating path. The above equation reveals that the scattered mmWave response has frequency shift related to the cardiac EM field on different frequency components, which can be expressed as:

$$C(t) = \sum_L A_t e^{j2\pi f_t} \beta_L(t), \tag{3}$$

where $C(t)$ is the CaSE response, A_t and f_t are the amplitude and frequency of the mmWave, respectively. Having modeled the CaSE, we next elaborate on the interrogation approach of CardiacWave.

5.2 CardiacWave Interrogation

The first step to sense cardiac electrical activity is to obtain a CaSE presentation of good quality using appropriate mmWave properties: **(1) Waveform**. Considering the continuity of cardiac activity monitoring, continuous wave is preferred. The single-tone continuous wave is not used because it cannot provide the required multiple frequency components for frequency shift analysis. Consequently, we adopt frequency-modulated continuous wave (FMCW) as the waveform of interrogation. **(2) Frequency**. In order to enhance the CaSE, higher frequency is preferred as the Verdet constant in β (Eq. (2)) will be larger [42]. However, mmWave with a frequency higher than 100 GHz attenuates fast and often requires expensive devices. CardiacWave uses 76 GHz that is supported by various commercial products [2] to gain a balance between sensing capability and cost. During interrogation, the probe emits the mmWave towards chest. The incoming mmWave is scattered from chest and its frequency is changed due to the CaSE. Then, the response containing cardiac EM field information is captured by the receiving probe. Finally, the received signal is sent to preprocessing followed by feature extraction.

5.3 Pre-processing

5.3.1 Response 2D demodulation. Given the *time-varying* mmWave response, it is crucial to have both the time and the frequency domains for further processing. Thereby, we utilize the short-time Fourier transform to demodulate the response. The mmWave signal captured by the probe will be divided into a series of small windows, which guarantees an appropriate time and frequency-domain resolution for each spectrogram. After the division, signals in these small windows will be transformed. Formally, the 2D demodulation outputs a *response matrix* $C = [C'_1(\omega), C'_2(\omega), \cdots, C'_m(\omega)]$. Each column can be formulated by

$$C'_m(\omega) = \sum_{n=-\infty}^{\infty} C[n]w[n-mR]e^{-j\omega n}, \tag{4}$$

where the w is the Hamming window to provide higher Signal-to-noise ratio (SNR), R is the step size between two successive windows. Here we set step size and window size as the time length of one FMCW chirp for adequate time and frequency domain resolution, respectively.

5.3.2 Body movement noise suppression. The response matrix C contains not only the CaSE response but also the noise components come from the direct mmWave reflection on human chest and other even other body areas, *i.e.*, body movement noise. As the FMCW waveform for CardiacWave interrogation uses sweeping frequency, the reflection and multi-path effect will finally form multiple high-energy noise peaks [45] on each column of the response matrix ($C'_m(\omega)$). To improve the SNR, the peaks need to be eliminated. CardiacWave leverages the constant false alarm rate (CFAR) method [52] for noise detection and elimination. For a specified false alarm rate p_{noise} (*i.e.*, the rate that a non-noise frequency component is detected as a noise peak), CFAR can maximize the noise detection probability according to the Neyman–Pearson lemma [56]. In particular, CFAR applies a moving average filter $W_{\text{CA}}(\cdot)$ for each column of the response matrix. Then, a threshold matrix σ is calculated by

$$\sigma = W_{\text{CA}}(C) \cdot |W_{\text{CA}}| \cdot ((p_{\text{noise}})^{-\frac{1}{|W_{\text{CA}}|}} - 1), \tag{5}$$

where $W_{\text{CA}}(C)$ is the filtered response matrix, $|W_{\text{CA}}|$ is the length of the moving average filter. For any element c in C that is greater than the corresponding element $\sigma(c)$ in σ, we consider c as a noise peak and set $c = \sigma(c)$. We empirically choose $p_{\text{noise}} = 0.001$, $|W_{\text{CA}}| = 8$ (see Section 7.4).
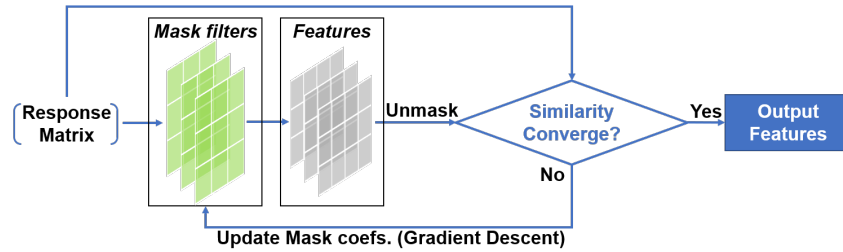
5.4 CaSE Mask-based Feature Extraction

Fig. 5. CardiacWave feature extraction.

CardiacWave utilizes the frequency shifts induced by the cardiac EM field to sense the cardiac electrical activities. Given the two-dimension (*i.e.*, the time and frequency domain) response matrix, a properly designed mask filter should be capable to extract the CaSE feature from the frequency shift to represent the cardiac electrical activity information. However, the response matrix is totally different from the 2D image in terms of physical model. This key difference rejects most existing mask filters designed for graphics, *e.g.*, the Sobel mask [68] for edge detection. Therefore, we employ mask filter with learnable coefficients, of which the mechanism is illustrated in Figure 5. Particularly, we randomly initialize multiple masks to filter the CaSE response to get initial features. The features are not representative at this time because the mask coefficients have not been learned yet. Then, we try to recover the response matrix from the features via unmask operations [61] as representative features should carry enough information of the CaSE response [10]. This step can be formulated as

$$g = \arg\min_{g,G} \text{MSE}(C, G(g(C))), \tag{6}$$

where g and G are coefficients of mask filters and unmask operators, respectively. MSE is the mean square error function. Since mask filter and unmask operation are differentiable in terms of the recovery error MSE, we are

able to update the mask coefficients via gradient descent [55]. Once the mask coefficients are learned, we use the updated masks to extract the CaSE features. We visualize the data generated by each step of the sensing scheme in Figure 6. It is clear from the visualization that the noise due to chest movement is eliminated and different CaSE features are learned. To provide enough ability to capture various minor frequency shift, CardiacWave uses 3×3 as the mask size and 64 as the number of the masks.
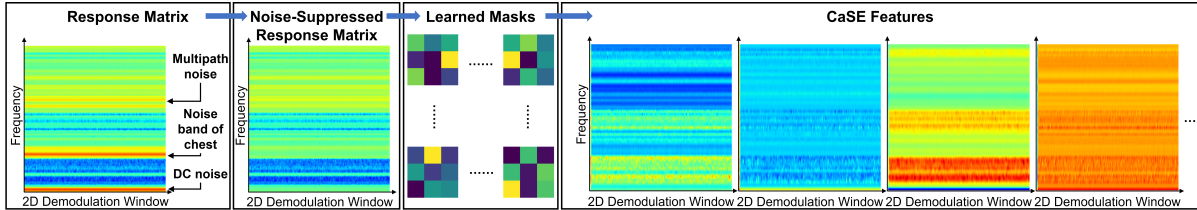

Fig. 6. Data visualization of each signal processing step in the entire CardiacWave sensing scheme.

6 CARDIAC ACTIVITY PROFILING

6.1 Solving CaSE-ECG Coupling

As described in Section 5.1, CaSE is caused by the cardiac EM field, whose root is the cardiac electrical activity. To profile cardiac electrical activity and get ECG records, it is important for us to understand how CaSE and ECG are coupled together. According to the Eq. (1), the H field is excited by the source element $J(\hat{t})$, which is revealed to be dependent on the ionic concentration in cardiac cells by cardiac electrophysiology:

$$J(\hat{t}) = \frac{\gamma T}{zF} \ln \left(P_K \frac{a_o^K}{a_i^K} + P_{Na} \frac{a_o^{Na}}{a_i^{Na}} + P_{Cl} \frac{a_o^{Cl}}{a_i^{Cl}} \right), \tag{7}$$

where γ is the gas constant, T is the absolute temperature, z is the valence of the ion, F is the Faraday constant, P is the permeability to the ion, and a_i, a_o are the concentration of the ion inside and outside the membrane, respectively [53]. The summation over $J(\hat{t})$ in all locations (represented by indexes i, j, k) forms the ECG signals [13], which can be formulated as:

$$\text{ECG}(t) = -\sum_{i,j,k} \frac{\vec{D}(t) \cdot \vec{r}}{r^3}, \vec{D}(t) \propto \nabla J(\hat{t}), \tag{8}$$

where $\vec{D}$ is dipole proportional to the gradient of $J(\hat{t})$ and $\vec{r}$ represents the distance between the cardiomyocytes's location and the ECG measurement point. The Eqs. (1)-(3), (7), and (8) together show the whole picture of CaSE-ECG coupling and forms a *partial differential equation system (PDEs)*, by solving which we are able to get ECG signals. A typical approach to deal with complex PDEs is using the finite element method for a numeric solution [59]. Nevertheless, the finite element method requires a large amount of computation and the calculated solution will be no longer valid when the conditions change. Accordingly, CardiacWave solve the CaSE-ECG coupling by data-driven deep neural networks (DNN), which recently show its power on solving PDE modeled problems efficiently [47]. Figure 7 shows the overarching design thinking and the stack of the cardiac activity profiling module. In the rest of this section, we detail the two specific designs that make the module.
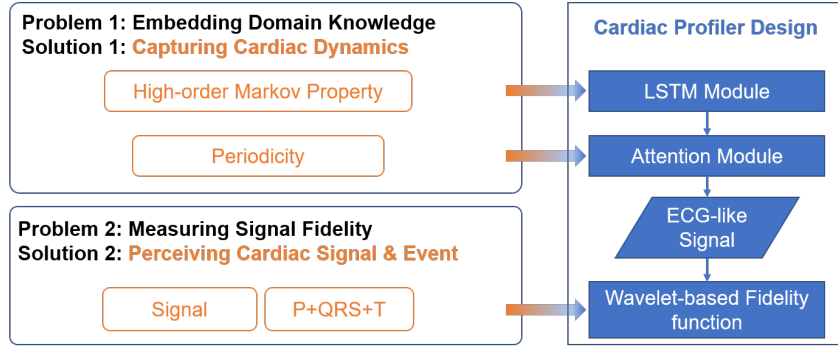
Fig. 7. CardiacWave's DNN-based activity profiler and the design thinking.

6.2 Capturing Cardiac Dynamics

The most intuitive question to develop the data-driven solver (*i.e.*, the cardiac activity profiler) is how to design the DNN architecture to learn the mapping between CaSE and ECG signal from the data. Most of the successful DNN models are developed for text (*e.g.*, BERT [21]) or image processing (*e.g.*, ResNet [28]). On the contrary, models for signal mapping across sensing modalities are still lacking. According to the NFL theorem [71], a model specifically designed for the problem can provide better approximation than generic models by introducing *domain knowledge*. In particular, Eq. (7) indicates that the source element $J(\hat{t})$ depends on the ionic concentration, which can be effectively modeled by discrete-time Markov formalism, according to cardiac dynamics researches [23, 30]. As the Markov property resides in the root of the CaSE and ECG, we construct a temporary neural network module that can capture the signal temporal properties (high-order Markov property) to retrieve integral information from CaSE features. More specifically, we adopt the recurrent neural network (RNN) design. Long Short Term Memory (LSTM) [32] is used to capture the high-order Markov property as:

$$\text{FoldR}(CELL, [0, \mathbf{C}_0, \cdots, \mathbf{C}_t]), \tag{9}$$

where $\mathbf{C}_t$ is the concatenation of the t-th columns of all CaSE feature matrixs and *CELL* is the LSTM cell. *CELL* can be regarded as a function closure that takes (hidden_state, cell_state) and CaSE feature, and returns (hidden_state', cell_state'). FoldR is a high-order function that can recursively apply *CELL* on the combination list. Compared to Gated Recurrent Unit [16], LSTM can provide higher reconstruction capacity.

Although LSTM is capable of draining the information in CaSE feature leveraging the Markov property, it cannot deal with the periodicity information, because both mmWave interrogation and ECG are signals of high sampling rate, *i.e.*, numerous data points are required to show periodicity. In this case, LSTM suffers from gradient vanishing during the optimization [31]. Therefore, we use the attention mechanism [75] to retrieve the long-term heart activity information. The attention mechanism can be formulated by

$$Attention(Q, K, V) = \text{Softmax}\left(\frac{QK'}{\sqrt{d_k}}\right)V, \tag{10}$$

where Q is queue matrix, K is key matrix, V is value matrix, d_k is the dimensions of query and key vector. We set $Q = K = V$ as the LSTM output so that the attention mechanism can capture the periodicity information of cardiac activity in a larger time scale.

6.3 Perceiving Cardiac Event

The DNN design based on the cardiac dynamics is driven by pursuing the reconstructed ECG-like signal with the maximum fidelity. Therefore, the target function describing the fidelity (fidelity function here after) plays an important role in CardiacWave's activity profiler. In ECG reconstruction, we not only focus on the global average distance between the reconstructed signal and the ground-truth ECG, but also the local cardiac event that is valuable in clinic. As the most widely used Mean Squared Error (MSE) usually flattens the peaks and valleys of the signal, we propose to use the distance between Discrete Wavelet Transform (DWT) coefficients [7] as the fidelity function. Specifically, we consider symlet wavelet [7], which balances the support width and vanishing moment and has good regularity to detect peaks and valleys effectively. In addition, it helps to avoid the influence of noise on the ECG signal. Thereby, the fidelity function in CardiacWave is defined as the 1-norm of DWT coefficients:

$$\mathcal{L}_w = \frac{1}{N} \sum_{i=1}^{N} (\mathcal{T} x_i - \mathcal{T} y_i), \mathcal{T} = \sum_{k=-\infty}^{\infty} x[k] f[2n-k], \tag{11}$$

where x_i is the ith data generated by the profiler, y_i is the ith ground truth ECG data, $\mathcal{T}$ is the DWT coefficients. f could be a high-pass filter or a low-pass filter to perceive cardiac events and signal distance.

7 CARDIACWAVE PROTOTYPING AND EVALUATION SETUP

7.1 Prototype Design

To achieve integral sensing of CaSE, CardiacWave choose the 4 GHz bandwidth ranging from 77 GHz to 81 GHz that provides enough room for capturing the CaSE-induced frequency shift. Many off-the-shelf mmWave probes are capable of generating the required mmWave. We adopt the Texas Instruments AWR1642Boost [3] for prototyping. We set the probe chirp period as 50 μs and the sampling rate as 256 samples per chirp. The idle time among chirps is 150 μs. The above specifications result in a 5000-Hz interrogation rate of the cardiac EM field. Then, we down-sample the interrogation to 500-Hz using nearest interpolation. During the experiment, we set the Rx gain as 30 dB and use a single TX and RX antenna. With this setting, the power consumption of the mmWave probe is around 9 W.

7.2 Evaluation Setup

7.2.1 Experiment preparation. We conduct extensive experiments to examine the capability of CardiacWave for cardiac monitoring. As shown in the Figure 8, the experimental setup can be divided into the *ECG part* (left) and the *mmWave part* (right). For *ECG part*, a subject is asked to sit in a chair in a relaxed position. We use off-the-shelf ECG Development Kit [58] (Shimmer 3^{TM}, hereafter, Shimmer ECG) to measure the subject's ECG signal at 500 Hz as the ground truth. Specifically, four limb electrodes are attached to the subject, forming three ECG channels, *i.e.*, channels I (LA-RA), II (LL-RA), and III (LL-LA). The RL is used as the reference electrode. For *mmWave part*, we align the mmWave probe in the direction of the subject's chest center to continuously sense the cardiac EM field. The subject orientation is 0° with respect to the probe, and the distance between the subject and the probe is 1 m. The mmWave signals are sent to the laptop with a 100-Mbps network adapter via RJ45 jack for recording. The training processes are done by an Nvidia Titan Xp graphical card with Pascal architecture [4].

7.2.2 Data Collection and Partition. The proposed study is approved by our institutional review board. In this study, we recruit 40 healthy subjects (*i.e.*, 20 males and 20 females) with their ages from 18 to 52 using email advertisements. Their weights are in the range of 45 kg to 84 kg. For each of them, we collect 10-minute ECG signals and reflected mmWave signals simultaneously. Both signals are synchronized to the clock on data gathering laptop. As for segmentation, the sample size is set to 500 data points (one second) and we empirically choose a 50% overlap (500 ms) between two adjacent samples. According to the segment length, we finally collect
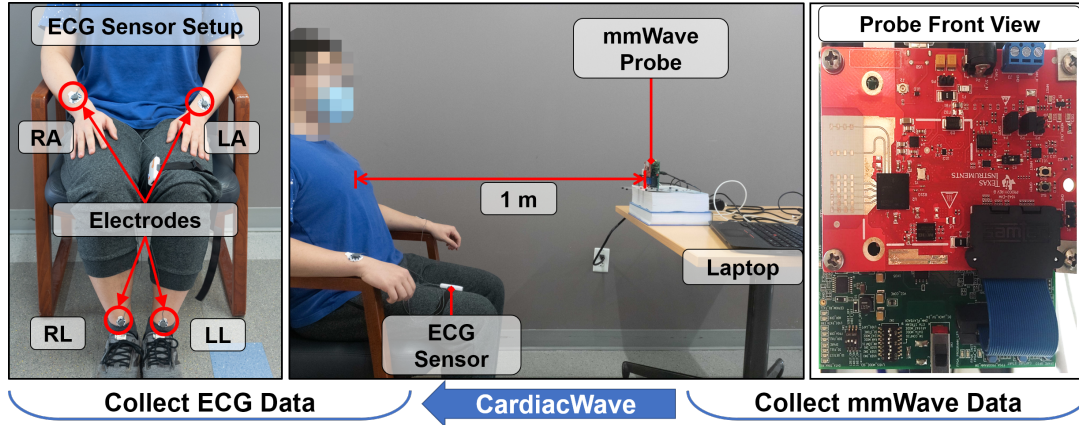
Fig. 8. The evaluation setup. Left: the ground-truth ECG sensor and its leads; Middle: subject's relative position; Right: the CardiacWave sensing probe.

47960 samples. We randomly select 30 subjects and use their samples (35876, 75%) for training, and the samples from the rest subjects are used for testing. The trained model is used in the following experiments by default unless otherwise stated.

7.3 Evaluation Metrics

7.3.1 Activity Event Integrity. **(1) Normalized Error**. The CardiacWave reconstructed signals (we use reconstructed ECG-like signals or ECG′ interchangeably) are expected to have integral cardiac events to enable heart electrical activity computing. As shown in the Figure 1, the modern ECG cardiac event system involves three principal components, which are P wave, QRS complex, and T wave [19]. Similar to RF-SCG [26], we use the normalized error of these components as a metric (*i.e.*, $\mathbf{P_{Err}}$, $\mathbf{QRS_{Err}}$, and $\mathbf{T_{Err}}$), which is the normalized difference between the *reconstructed ECG-like timing* and the *ECG baseline timing*, formulated as:

$$\text{Err} = \frac{|\text{CardiacWave Reconstruction} - \text{ECG Baseline}|}{\text{Heartbeat duration}} \tag{12}$$

Besides, the time elapsed between R-waves of two successive QRS complexes (R-R interval) is associated with respiratory sinus arrhythmia [44], diabetes [12], and mental disorders such as insomnia [60]. Additionally, the time elapsed between the start of the QRS complex and the end of the T wave (Q-T interval) has been adopted as the major indicator of ventricular pro-arrhythmicity [73]. Therefore, we propose to measure the normalized error of Q-T interval ($\mathbf{QT_{Err}}$) and the R-R interval ($\mathbf{RR_{Err}}$) per cardiac cycle between the reconstructed ECG-like signal and ECG baseline to evaluate the cardiac event integrity. All the timings are labeled based on the channel I signal and synchronized to other channels. **(2) Weighted Event Distortion (WED):** WED is a integrated events distortion highly correlated with experts' visual inspect and opinion according to studies [49, 79, 80] in the field. The WED can be calculated as:

$$\text{WED}(\text{ECG}, \text{ECG}') = 100\Delta\vec{\mathcal{E}}^T \times \frac{\text{diag}(\phi)}{\text{trace}(\text{diag}(\phi))} \times \Delta\vec{\mathcal{E}},$$

$$\Delta\vec{\mathcal{E}} = [\frac{|\mathcal{E}_i^{ECG} - \mathcal{E}_i^{\text{ECG}'}|}{\max(\mathcal{E}_i^{ECG}, \mathcal{E}_i^{\text{ECG}'})}], i \in [1, 10] \tag{13}$$

where ϕ represents weights, $\Delta\vec{\mathcal{E}}$ is the cardiac event feature vector detailed in Table 1, diag($\cdot$) and trace($\cdot$) are diagonal matrix and trace functions. ϕ is set to [2 1 1 1 1 1 2 2 1 1] to better fit cardiologists' opinion [80]. Typically, reconstructed ECG-like signals with WDD in range [0, 12], (12, 18], (18, 40] are considered to be "**Good**", "**Not Good**", and "**Bad**" [8], respectively.

Table 1. Cardiac event features [80] used for WED calculation.

Cardiac Event Features	Description
Duration-based feature	**the duration between ...**
$\mathcal{E}_1$: cardiac cycle	two successive R peaks
$\mathcal{E}_2$: ventricular depolarization	the start and the end of QRS complex
$\mathcal{E}_3$: entire ventricular systole	the start of the QRS complex and the end of T wave
$\mathcal{E}_4$: ventricular isovolumetric contraction	the start of the QRS complex and the T peak
$\mathcal{E}_5$: atrial depolarization	P wave
$\mathcal{E}_6$: AV node conduction	the start of P wave and the start of QRS complex
Strength-based features	
$\mathcal{E}_7$: ventricular capacity	The maximum positive amplitude of QRS complex
$\mathcal{E}_8$: interventricular septum depolarization	The minimum negative amplitude of QRS complex
$\mathcal{E}_9$: atrial contraction	The amplitude of P wave
$\mathcal{E}_{10}$: cardiac sympathetic nervous excitation	The amplitude of T wave

7.3.2 Signal Fidelity. As cardiac electrical activity has been discovered to have more implicit information, such as emotional and identity information, it is vital to reconstruct high-fidelity ECG signals for facilitating further heart activity computing. We use **cross-correlation (Corr)** [49] and **signal-to-noise ratio (SNR)** [51] to evaluate the reconstructed ECG-like signals from the perspective of fidelity. Corr is a measurement of signal similarity widely used in signal processing. It has the following form when we compare the reconstructed ECG-like signal with the ECG baseline:

$$\text{Corr} = (\text{ECG}' \star \text{ECG})[\tau] = \sum_{j=-\infty}^{\infty} \text{ECG}'[j]\text{ECG}[j+\tau], \tag{14}$$

where parameter τ is the displacement. As ECG' $\star$ ECG is a curve with regards to τ, the auto correlation of the ground truth (AutoCorr), *i.e.*, ECG $\star$ ECG is used as benchmark. Additionally, the cross-correlation coefficient (normalized Corr) is adopted to give a quantitative evaluation of the reconstructed ECG-like signals. Reconstructed signals with high fidelity would give a Corr close to the benchmark. In addition, considering CardiacWave is a novel cardiac monitoring scheme with sensor-like architecture, it is natural and important to evaluate the fidelity of the reconstructed ECG-like signals in terms of sensing SNR. Notably, we understand the noise as the difference between the ECG and the ECG' (which is widely adopted in ECG quality evaluation [8, 18, 51]). Thereby, the SNR is formulated as:

$$\text{SNR}_{dB} = 10 \log_{10} \left(\frac{\sum_n [\text{ECG}[n] - \overline{\text{ECG}}]^2}{\sum_n [\text{ECG}[n] - \text{ECG}'[n]]^2} \right). \tag{15}$$

7.4 System Calibration

We conduct system calibration to observe the influence of the noise suppression parameter W_{CA} and p_{noise} to the system and empirically determine the parameter value for the following evaluation. In detail, we use SNR_{dB} as the metric of the sensing noise. We observe the mean SNR_{dB} with p_{noise} being set to 0.1, 0.01, 0.001, and 0.0001,

respectively. For each setting of p_{noise}, the W_{CA} ranges from 8 to 32. The results reported in Figure 9 show that when the $p_{noise} = 0.001$ and $W_{CA} = 8$, the CardiacWave has best performance on SNR_{dB}. With the increasing of the W_{CA}, the SNR_{dB} decreases as large moving windows may dilute the CaSE information.
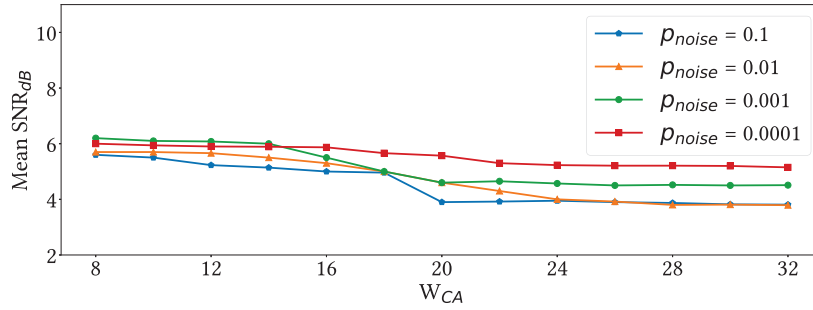

Fig. 9. The mean SNR_{dB} of CardiacWave with different settings of W_{CA} and p_{noise}.

8 CARDIAC EVENT INTEGRITY

To evaluate the cardiac event integrity, we leverage an automated ECG analysis algorithm [6] over the testing data to label the cardiac event features. We first calculate the average accuracy of the three ECG principle components over all the testing data and show the result in Figure 10. The normalized error of P wave, T wave, and QRS complex is observed as 0.67%, 0.71%, and 0.49%, respectively. The corresponding cardiac event difference is 6.1 ms, 4.2 ms, and 5.7 ms, respectively. We note that the error of the QRS complex is lower than that of the other two components. One reason for the better performance of QRS complex reconstruction is the QRS complex has a sharp peak that can be easily perceived by the DWT-based fidelity function. This phenomenon also reveals that the CardiacWave event integrity could be further improved in the future by using the newly discovered better fidelity function.
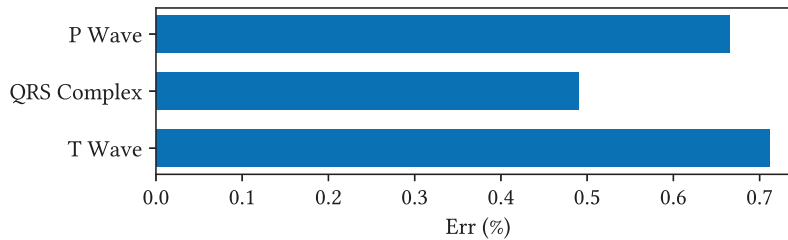

Fig. 10. The normalized error of CardiacWave in terms of T wave, QRS complex, and P wave.

Then, we calculate the normalized error of the R-R interval and Q-T interval. As observed in Figure 11, the RR_{Err} of 50% reconstructed ECG-like signals range from 0.14% to 0.75%, while the QT_{Err} of 50% reconstructed ECG-like signals range from 0.27% to 1.16%. To be specific, the mean value of RR_{Err} and QT_{Err} are around 0.51% and 0.91%, respectively. Overall, CardiacWave achieves better performance in reconstructing R-R interval compared with
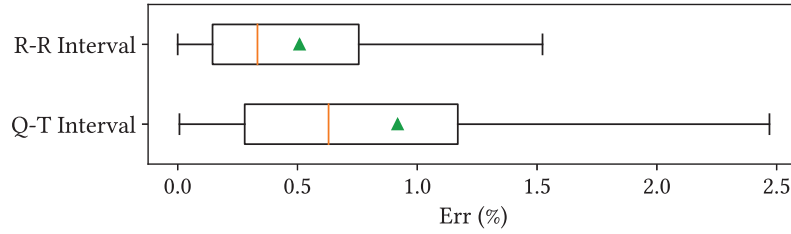
Fig. 11. The normalized error of CardiacWave in terms of Q-T interval and the R-R interval.

that of Q-T interval. The reason behind this is two-fold. First, as a part of the QRS complex, the R peak can be easily perceived by the fidelity function. Second, the R peak causes a stronger CaSE response because the R peak is the most vigorous cardiac electrical activity that pumps blood to the human body.

To further analyze the normalized error distribution of R-R interval and Q-T interval reconstructed by CardiacWave, we report the accumulated frequency of RR_{Err} and QT_{Err} in Figure 12. We observe that 95% of the reconstructed ECG-like signals are with $RR_{Err} < 1.28\%$ and $QT_{Err} < 2.57\%$, which is a strong indicator that CardiacWave can provide superior cardiac activity event integrity. By preserving accurate Q-T and R-R interval information, the ECG-like signals reconstructed by CardiacWave show the great potential to help the diagnosis of a series of physical and mental disorders, such as sinus arrhythmia, diabetes, and insomnia [12, 44, 60].
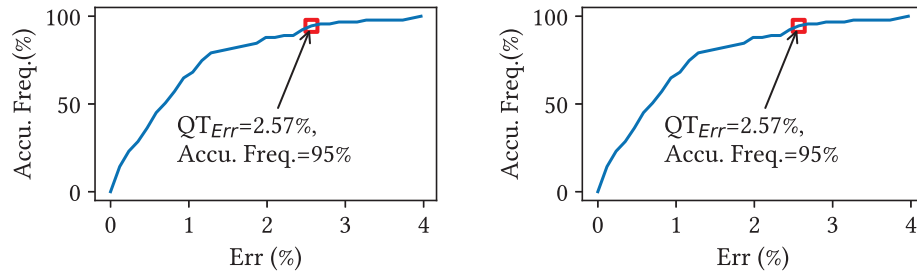

Fig. 12. The accumulated frequency of RR_{Err} and QT_{Err} in CardiacWave.

Furthermore, we report the Weighted Event Distortion (WED) in Figure 13 to demonstrate CardiacWave's integrity from the time duration and amplitude perspectives (features are detailed in Table 1). As observed in Figure 13, the reconstructed multi-channel ECG-like signals report "**Good**" quality in terms of WED, where the mean WED of channels I, II, and III are 6.15 (std=2.41), 7.05 (std=2.95), and 6.24 (std=3.33), respectively. These results reveal that not only Q-T and R-R interval features of the reconstructed ECG signals are integral, but also their various cardiac event features are good to the cardiologist for reference. We observe the WED of channel II is slightly greater than the other channels, the reason behind which might be the channel II signal has a lower amplitude. This implies the performance on channel II can be further improved by applying normalization [62].
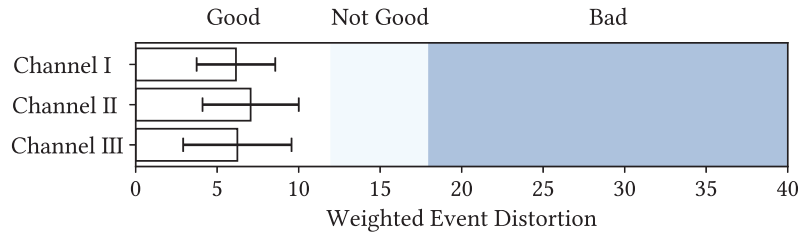
Fig. 13. The weighted event distortion of CardiacWave.

9 SIGNAL FIDELITY

Figure 14 shows a five-cardiac-cycle reconstructed ECG-like spectrum by CardiacWave and the corresponding ECG measurement (baseline) of one subject. The reconstructed ECG-like signals present the same periodicity compared with the ECG baseline in Channel I, II, III. In each cardiac cycle, the local maximum and minimum of reconstructed signals are close to those of the baseline. The slight misalignment randomly happens in these three channels from our observation. To summarize, CardiacWave is feasible to reconstruct visually accurate ECG data. With this basic sense of the CardiacWave performance, we then quantitatively evaluate the fidelity of the reconstructed ECG-like signals by the correlation and the SNR.
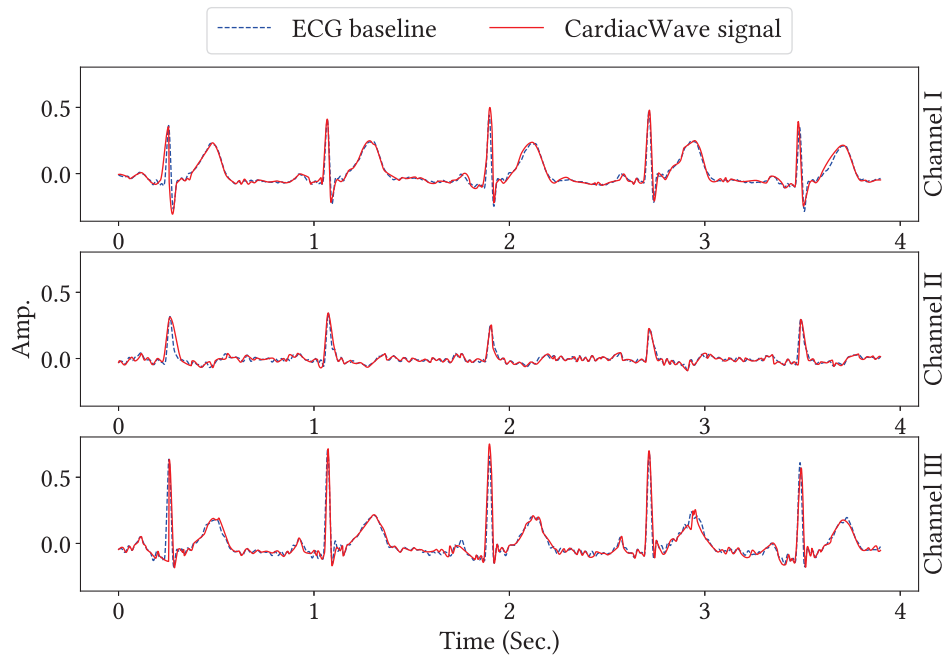

Fig. 14. The comparison between CardiacWave reconstructed signals and the corresponding ECG baseline among Channel I, II, III.

We conduct the correlation analysis between 10-second reconstructed ECG-like signals and their corresponding ECG baseline. As shown in Figure 15, the mean correlation coefficients of Channel I, II, and III are 0.901, 0.892, and 0.913, respectively, with the standard deviation being around 0.06. The p-values for these channels are all less than 0.0001, which suggests the significance of the finding. Therefore, we can conclude that the reconstructed ECG-like signals yield a strongly positive correlation with the ECG baseline.
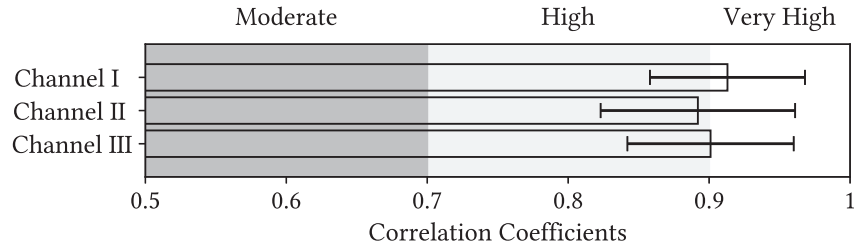

Fig. 15. The correlation coefficients between CardiacWave reconstructed signals and the corresponding ECG baseline among Channel I, II, III.

Further, the quantitative SNRs are evaluated and shown in Figure 16. The mean SNR of reconstructed ECG-like signals in Channel I, II, and III are 6.07, 5.79, 5.07 dB, respectively. The minimum SNR values in these three channels are all above 3.7. The accumulated frequency curve in Figure 16 depicts the distribution of SNR. We observe that 95% of reconstructed ECG-like samples are with SNR>5 for Channel I, SNR>4.75 for Channel II, and SNR>4.25 for Channel III. The above observations indicate the superior fidelity of the reconstructed ECG-like data by CardiacWave.
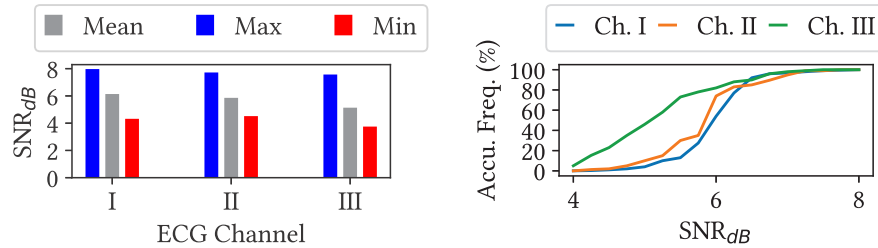

Fig. 16. Left: the SNR performance of CardiacWave in Channel I, II, III; Right: the accumulated frequency of SNR in Channel I, II, III.

Summary. CardiacWave offers satisfying integral clinical characteristics and signal fidelity in the evaluation in Sections 8 and 9. Besides, we notice that the WED will raise up to 300% when we use conventional MSE loss as the fidelity function. This is because the cardiac event perceiving in the activity profiler can significantly capture the fiducial points such as P, T, and R peaks. Meanwhile, the SNR decreases 3.3 dB on average when we leverage mmWave interrogation without applying noise suppression, which demonstrates our proposed noise-resistant sensing scheme can help acquire more integral and fidelity heart information. Therefore, we can summarize that

the developed sensing scheme and cardiac activity profiler meet the design targets, and CardiacWave has a good capability to monitor high-definition heart electrical activities in a non-contact manner. In the following two sections, we analyze the usability and the robustness of CardiacWave, respectively.

10 USABILITY ANALYSIS

10.1 Impact of Heart & Breath Rate Variability.

In different situations, users' heart and breath rates may vary due to physical/social activities. This motivates us to explore whether heart and breath rate variation will degrade CardiacWave's performance. We invite three subjects from the testing group to participate in this experiment. As breathing is easier to control and will affect heart rate, we first explore the impact of heart rate variability without breathing influence. The participants are asked to do sports to raise their heart rates to 150 beats per minute (BPM) or above. Then, their ECG and ECG′ were measured continuously with the same setup in Sections 7.2, until their heart rates fall below 100 BPM. Notably, participants are asked to hold breath when their heart rates are around 140, 120, and 100 BPM so that the influence of breath is controlled. The mean QT_{Err} and RR_{Err} of the reconstructed ECG-like signals are depicted in Figure 17. From 100 to 140 BPM, the mean QT_{Err} are 0.83%, 0.82%, and 0.79%, and the mean RR_{Err} are 0.58%, 0.57%, and 0.54%. Next, the participants are requested to take 15, 20, 30 breaths per minute and last for 2 minutes with the help of a stopwatch, where the configuration "15 breaths per minute" is close to the resting status and needs less effort to control. As shown in Figure 17, the mean QT_{Err} are 0.83%, 0.81%, and 0.82%, and the mean RR_{Err} are 0.60%, 0.57%, 0.61%, respectively.
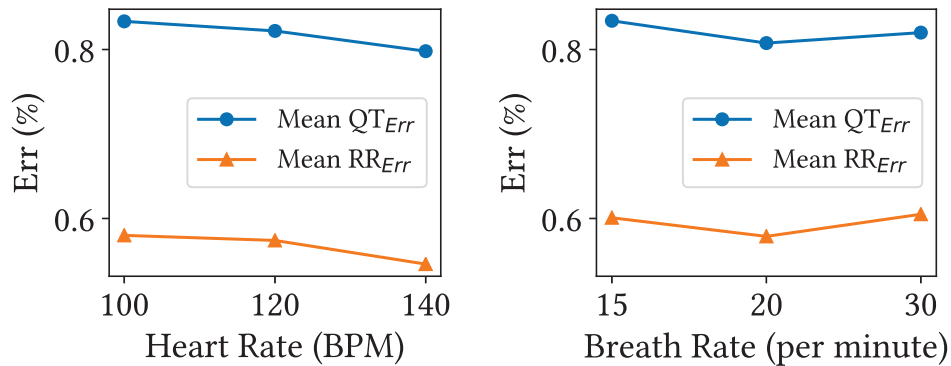

Fig. 17. The QT_{Err} and RR_{Err} performance of CardiacWave with different heart and breath rates.

Insight. The curves of QT_{Err} and RR_{Err} show a slight decrease when the heart rate increases. The reason is that the cardiac activity becomes more vigorous as the heart rate increase. The vigorous cardiac activity enhances the CaSE response. Moreover, the events are perceived more easily due to the increase of ECG amplitude. We believe the slight decrease when the rate is 20 breaths per minute is because the heart rate fluctuates when the participants make more efforts to control their breath rate. The participants also confirmed that 20 breaths per minute is harder to achieve compared with the other two breathing rates. These results indicate the CardiacWave has a strong tolerance to heart and breath rates variability.

10.2   Impact of Tobacco Use.

Tobacco strongly influences the heart's functionality. There are over one billion people who use tobacco [5] around the world and more than 30% of the non-smoker were exposed to secondhand smoke [1]. To enable potential application in healthcare, CardiacWave should have no performance decrease on people who use tobacco. We recruit two participants who used tobacco within one day and collect 10-minute ECG ground truth and RF ECG data. As observed in Figure 18, the WED of reconstructed ECG-like data from tobacco and non-tobacco user is 7.69 and 7.62, respectively.
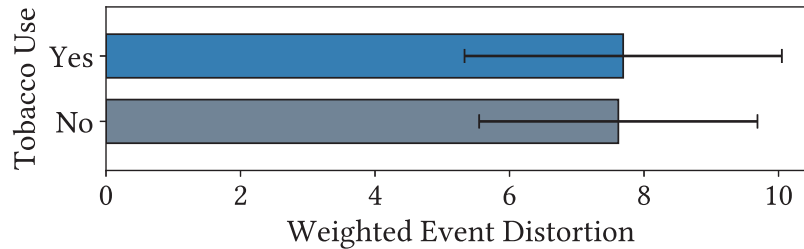

Fig. 18. The WED performance of CardiacWave with tobacco usage.

Insight. The WED of reconstructed ECG-like data from tobacco and non-tobacco user locates in the range "**Good**" and the performance of CardiacWave appears to be unaffected by tobacco use. While Nicotine and other ingredients in tobacco may affect the iron concentration in cardiac cells [15], we believe the intrinsic CaSE-ECG coupling is much less influenced since the electromagnetism relation between CaSE and ECG remains unchanged.

10.3   Impact of Age.

CardiacWave is expected to have no bias on different age groups as a novel heart activity computing scheme. In this experiment, we divide the testing participants into five age groups and recruit five extra participants so that each group has three participants. All the experimental setup is the same as we mentioned in Section 7.2. As shown in Figure 19, the WED of reconstructed ECG-like data from the five age groups are around 6.7, which can be considered as "**Good**".
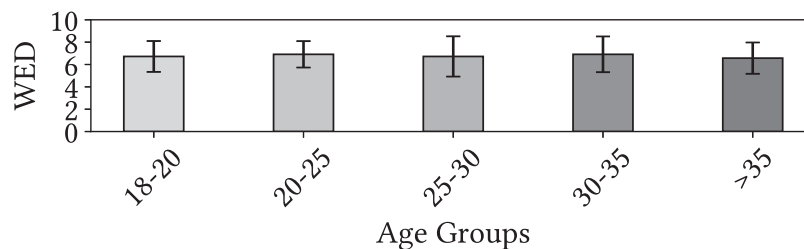

Fig. 19. The WED performance of CardiacWave with different age groups.

Insight. The results illustrated in Figure 19 indicates that the CardiacWave performance will not be affected by age factor. Thereby, we anticipate that CardiacWave can largely benefit the old people who have the cardiac electrical monitoring requirements but have difficulties in setting up the electrodes.

10.4 Impact of Gender.

CardiacWave is also expected to have no bias between male and female. Here, we perform correlation analysis between reconstructed ECG-like signals and the baseline among 20 males and 20 females. No bias is observed in the results shown in the Figure 20. The mean correlation coefficients are 0.88 and 0.90 for males and females, respectively. The results are close to 1 and are considered to be highly positive correlation [50].
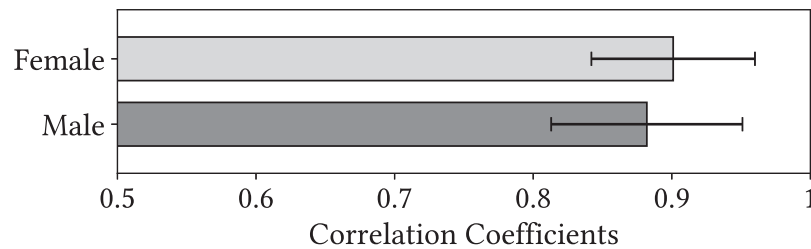

Fig. 20. The correlation coefficients of the reconstructed ECG-like signal for different genders.

11 ROBUSTNESS INVESTIGATION

11.1 Impact of Exercise.

CardiacWave is expected to facilitate heart electrical activity computing in various situations, especially the scenarios that are in demand but ECG cannot be applied, such as exercise. Especially, intense weightlifting may cause severe heart attack [22]. However, electrodes-based ECG monitoring is limited because the chest muscle excitation under this circumstance will dominate the ECG, resulting in an unstable heart activity recording [29]. Therefore, we are interested in if CardiacWave can facilitate heart electrical activity monitoring in this case. We invite a participant to do dumbbell lifting in front of the probe and record the RF ECG data and ECG baseline simultaneously. The distance between the participant and the probe is 1 m. The participant wears a XiaoMi band [33] to record the heart rate via PPG.
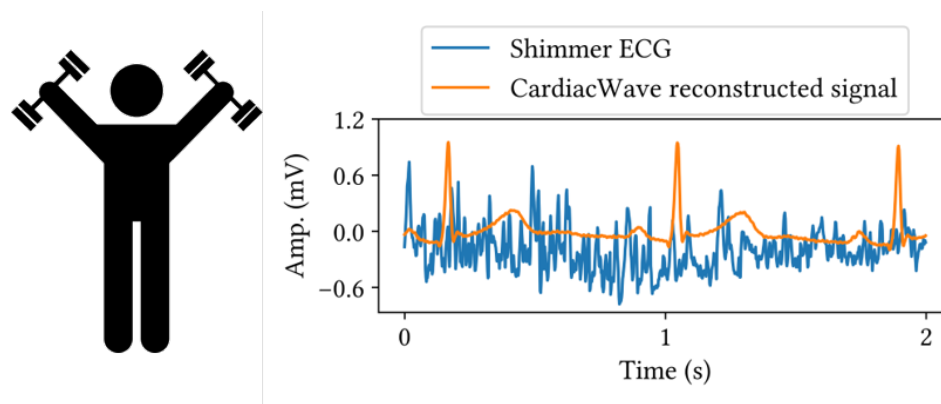

Fig. 21. CardiacWave is robust to dumbbell exercise whereas ECG is severely interfered by muscle excitation.

Insight. As shown in Figure 21, CardiacWave is capable to record heart's electrical activity. As the ECG in this scenario is corrupted, we compare the heart rate calculated by CardiacWave reconstructed signals with that reported by XiaoMi band and find that the difference is 3 BPM. To adapt to the exercise involving location changes, such as running, mmWave beamforming [26] can be integrated into the CardiacWave sensing scheme for target tracking.

11.2 Sensing Range & User Orientation.

Sensing range and user orientation are two key factors that influence the robustness of CardiacWave. CardiacWave should require minimum user cooperation and be tolerant to unfixed locations. Therefore, we conduct the experiments to examine the CardiacWave's performance under changeable sensing distances and human orientations. Specifically, five subjects are asked to sit align to the mmWave probe while the distance between the subjects and the probe is set from 1 m to 3 m with a 1-meter distance step. As shown in Figure 22, on each distance configuration, we have orientation configuration at 0°, ±30°, and ±60°.
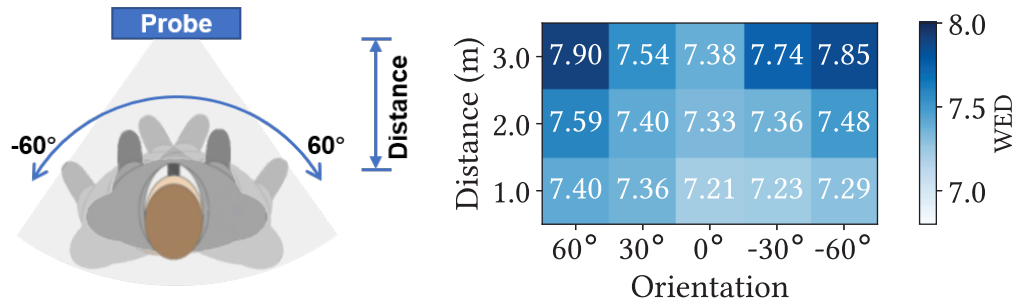

Fig. 22. The WED performance of CardiacWave with different sensing distances and orientations.

Insight. The results show the mean WED locates in the range from 7.21 to 7.90, which are considered to be good quality. We observe that the WED decreases slightly as the distance and orientation increase. The reason is that the attenuation of mmWave slightly decreases the SNR. The performance of the prototype under these circumstances could be further improved by integrating beamforming function.

11.3 Impact of Accessories.

Users may wear different kinds of accessories on demand in some cases. Therefore, we are curious about whether these wearable accessories can affect mmWave signals and lead to an unfavorable performance. The participants are requested to wear three commonly used accessories in this experiment, *i.e.*, a wool scarf, earpods with MIC, and a ballpoint pen fabricated by plastic and ink that can be attached to the chest pocket, respectively. Particularly, the MIC of the earpods is placed in front of the chest to test if the MIC-generated EM field will interfere with the CaSE. Figure 23 shows that the errors of P wave, T Wave, and QRS complex are around 0.50, 0.65, and 0.70.

Insight. The above results indicate that these three wearable accessories do not degrade the performance of the CardiacWave. As regards the scarf, the CaSE can not be shielded by the material because of the mmWave penetration. We observe that the CardiacWave's error faintly increases due to the earpods EM field interference. The field is relatively static and attenuates fast so that it can only interfere with a small part of the cardiac
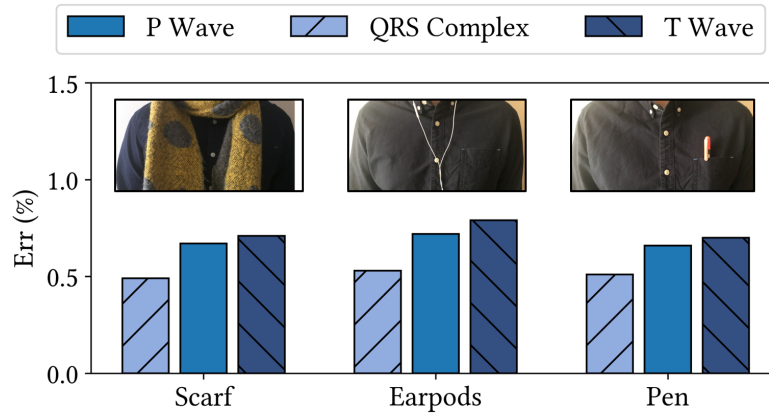
Fig. 23. The P_{Err}, QRS_{Err}, and T_{Err} performance of CardiacWave with different accessories.

EM field. By learning mask coefficients under the EM field interference, CardiacWave can further improve its robustness to ambient EM interference.

12 LIMITATION AND FUTURE WORKS

In this section, we discuss the limitations of CardiacWave and identify the future works of CardiacWave to forge a practical medical tool.

- **Cardiac States.** Cardiac system is a rather complex system coordinated by multiple parts and millions of cells. Considering the activities in daily life, CardiacWave can be evaluated in the future on varying cardiac states via rigorous protocol, such as cold-pressor [24]. Moreover, the malfunction of different parts results in distinct cardiac EM fields [27]. Future works can evaluate CardiacWave on cardiac disease patients and further determine the applicable range of CardiacWave. For the mentioned evaluations, a larger population could help to reduce bias [57].
- **Environmental variance.** Considering that the CaSE effect is based on the mmWave scattering of cardiac EM field, environmental variance such as EM leakage could influence the performance of CardiacWave. To adapt CardiacWave to different environments, an effective calibration mechanism is required. For most daily-life scenarios (*e.g.*, smart home health monitoring), we anticipate the multi-path effect is relatively static and only one calibration during the first-time deployment will be needed. In addition, spatial filtering technologies [20] can be used for better isolation of the CaSE effect in complex environments by increasing the SNR. As common customer electronics are designed with good EM compatibility [54], we remain the performance under EM leakage unevaluated. Yet, the impact of other high-frequency EM wave leakage sources like microwave ovens on performance should be explored and evaluated in future work.
- **System integration.** We anticipate CardiacWave can be seamlessly integrated into most indoor environments with continuous power supply, such as gyms and workshops to improve sports and occupational safety. Further researches on concurrent heart activities monitoring could help to reduce the number of the required hardware. For potential applications on mobile devices, how to integrate CardiacWave into mmWave baseband processor or other dedicated chips for better energy efficiency is still an open problem.

13 CONCLUSION

Existing non-contact cardiac activity monitoring solutions are limited by immature analysis tools for achieving fine-granularity cardiac characterization in healthcare applications. In this paper, we propose CardiacWave, a mmWave-based non-contact and high-definition heart electrical activity monitoring system to provide ECG-like heart activities measure, including P-waves, T-waves, and QRS complex. We first investigate the cardiac-mmWave scattering effect (CaSE), *i.e.*, the electromagnetic field caused by cardiac electrical activity can impact the chest-scattered RF signals. Based on it, we leverage the 76 GHz frequency-modulated mmWave to interrogate and demodulate the CaSE response. After noise suppression and mask-based feature extraction, we fed the integral CaSE descriptors to a deep neural network-based cardiac activity profiler for generating ECG-like signals. Experiment results show that the weighted event distortion of generated ECG-like signal is around 7, which indicates good cardiac event integrity. Also, CardiacWave measures have a high positive correlation with ECG baseline.

REFERENCES

[1] 2015. Second-hand smoke. https://www.who.int/gho/phe/secondhand_smoke/en/
[2] 2020. Global Millimeter Wave Radar IC Market Report Expected to Generate an Estimated $1.3 Billion by 2025 - ResearchAndMarkets.com. https://www.businesswire.com/news/home/20200203005440/en/Global-Millimeter-Wave-Radar-IC-Market-Report-Expected-to-Generate-an-Estimated-1.3-Billion-by-2025---ResearchAndMarkets.com
[3] 2021. mmWave sensors. http://www.ti.com/sensors/mmwave/overview.html
[4] 2021. NVIDIA TITAN Xp Graphics Card with Pascal Architecture. https://www.nvidia.com/en-us/titan/titan-xp/
[5] 2021. Tobacco. https://www.who.int/news-room/fact-sheets/detail/tobacco
[6] Nima Aalizade. 2021. ECG P QRS T wave detecting matlab code - File Exchange - MATLAB Central. https://www.mathworks.com/matlabcentral/fileexchange/66098-ecg-p-qrs-t-wave-detecting-matlab-code
[7] Paul S Addison. 2005. Wavelet transforms and the ECG: a review. *Physiological measurement* 26, 5 (2005), R155.
[8] Amjed S Al-Fahoum. 2006. Quality assessment of ECG compression techniques using a wavelet-based diagnostic measure. *IEEE Transactions on Information Technology in Biomedicine* 10, 1 (2006), 182–191.
[9] Urs Anliker, Jamie A Ward, Paul Lukowicz, Gerhard Troster, Francois Dolveck, Michel Baer, Fatou Keita, Eran B Schenker, Fabrizio Catarsi, Luca Coluccini, et al. 2004. AMON: a wearable multiparameter medical monitoring and alert system. *IEEE Transactions on information technology in Biomedicine* 8, 4 (2004), 415–427.
[10] Pierre Baldi. 2012. Autoencoders, unsupervised learning, and deep architectures. In *Proceedings of ICML workshop on unsupervised and transfer learning*. 37–49.
[11] R. Banerjee, A. Sinha, A. D. Choudhury, and A. Visvanathan. 2014. PhotoECG: Photoplethysmographyto estimate ECG parameters. In *2014 IEEE International Conference on Acoustics, Speech and Signal Processing (ICASSP)*. 4404–4408. https://doi.org/10.1109/ICASSP.2014.6854434
[12] Thomas Benichou, Bruno Pereira, Martial Mermillod, Igor Tauveron, Daniela Pfabigan, Salwan Maqdasy, and Frederic Dutheil. 2018. Heart rate variability in type 2 diabetes mellitus: A systematic review and meta–analysis. *PloS one* 13, 4 (2018), e0195166.
[13] Omer Berenfeld and Shimon Abboud. 1996. Simulation of cardiac activity and the ECG using a heart model with a reaction-diffusion action potential. *Medical engineering & physics* 18, 8 (1996), 615–625.
[14] Darrian Bryant, Sourabh Ravindran, Neeraj Magotra, and Steve Northrup. 2010. Real-time implementation of a chest-worn accelerometer based heart monitoring system. In *2010 53rd IEEE International Midwest Symposium on Circuits and Systems*. IEEE, 1057–1060.
[15] J Harold Burn. 1960. Action of nicotine on the heart. *Annals of the New York Academy of Sciences* 90, 1 (1960), 70–73.
[16] Junyoung Chung, Caglar Gulcehre, KyungHyun Cho, and Yoshua Bengio. 2014. Empirical evaluation of gated recurrent neural networks on sequence modeling. *arXiv preprint arXiv:1412.3555* (2014).
[17] JL Cruz, MV Andres, and MA Hernandez. 1996. Faraday effect in standard optical fibers: dispersion of the effective Verdet constant. *Applied optics* 35, 6 (1996), 922–927.
[18] S Dandapat, LN Sharma, and RK Tripathy. 2015. Quantification of diagnostic information from electrocardiogram signal: A review. In *Advances in communication and computing*. Springer, 17–39.
[19] Antoni Bayes De Luna. 2012. *Clinical Electrocardiography, Enhanced Edition: A Textbook*. John Wiley & Sons.
[20] Vittorio Degli-Esposti, Franco Fuschini, Enrico M Vitucci, Marina Barbiroli, Marco Zoli, Li Tian, Xuefeng Yin, Diego Andres Dupleich, Robert Müller, Christian Schneider, et al. 2014. Ray-tracing-based mm-wave beamforming assessment. *IEEE Access* 2 (2014), 1314–1325.
[21] Jacob Devlin, Ming-Wei Chang, Kenton Lee, and Kristina Toutanova. 2018. Bert: Pre-training of deep bidirectional transformers for language understanding. *arXiv preprint arXiv:1810.04805* (2018).

[22] Karim El-Sherief, Ali Rashidian, and Sundararajan Srikanth. 2011. Spontaneous coronary artery dissection after intense weightlifting UCSF Fresno Department of Cardiology. *Catheterization and Cardiovascular Interventions* 78, 2 (2011), 223–227.

[23] Martin Fink and Denis Noble. 2009. Markov models for ion channels: versatility versus identifiability and speed. *Philosophical Transactions of the Royal Society A: Mathematical, Physical and Engineering Sciences* 367, 1896 (2009), 2161–2179.

[24] Shadi Ghiasi, Alberto Greco, Riccardo Barbieri, Enzo Pasquale Scilingo, and Gaetano Valenza. 2020. Assessing autonomic function from electrodermal activity and heart rate variability during cold-pressor test and emotional challenge. *Scientific reports* 10, 1 (2020), 1–13.

[25] Robert P Grant. 1958. Clinical electrocardiography. *Academic Medicine* 33, 3 (1958), 242.

[26] Unsoo Ha, Salah Assana, and Fadel Adib. 2020. Contactless Seismocardiography via Deep Learning Radars. In *Proceedings of the 26th Annual International Conference on Mobile Computing and Networking* (London, United Kingdom) *(MobiCom '20)*. Association for Computing Machinery, New York, NY, USA, Article 62, 14 pages. https://doi.org/10.1145/3372224.3419982

[27] John Hampton. 2013. *The ECG in practice.* Elsevier Health Sciences.

[28] Kaiming He, Xiangyu Zhang, Shaoqing Ren, and Jian Sun. 2016. Deep residual learning for image recognition. In *Proceedings of the IEEE conference on computer vision and pattern recognition.* 770–778.

[29] InterMountain HealthCare. 2021. Holter Monitor Test. https://intermountainhealthcare.org/ckr-ext/Dcmnt?ncid=520670934

[30] Stefan Herzig, PARAG Patil, Joachim Neumann, Carl-Michael Staschen, and David T Yue. 1993. Mechanisms of beta-adrenergic stimulation of cardiac Ca2+ channels revealed by discrete-time Markov analysis of slow gating. *Biophysical journal* 65, 4 (1993), 1599–1612.

[31] Sepp Hochreiter. 1998. The vanishing gradient problem during learning recurrent neural nets and problem solutions. *International Journal of Uncertainty, Fuzziness and Knowledge-Based Systems* 6, 02 (1998), 107–116.

[32] Sepp Hochreiter and Jürgen Schmidhuber. 1997. Long short-term memory. *Neural computation* 9, 8 (1997), 1735–1780.

[33] Mi Global Home. 2021. Mi Band. https://www.mi.com/global/miband

[34] Yu-Jie Hsu, Chun-Hsiung Wang, Shu-Sheng Lee, Wen-Jong Wu, and Chih-Kung Lee. 2020. Non-contact PPG measurement system incorporating image analyzed photoplethysmogram signals and deep learning algorithms. In *Biophotonics in Point-of-Care*, Vol. 11361. International Society for Optics and Photonics, 113610C.

[35] J Willis Hurst. 1998. Naming of the waves in the ECG, with a brief account of their genesis. *Circulation* 98, 18 (1998), 1937–1942.

[36] Sinh Huynh, Rajesh Krishna Balan, JeongGil Ko, and Youngki Lee. 2019. VitaMon: measuring heart rate variability using smartphone front camera. In *Proceedings of the 17th Conference on Embedded Networked Sensor Systems.* 1–14.

[37] Hideo Iizuka, Kunio Sakakibara, Toshiaki Watanabe, Kazuo Sato, and Kunitoshi Nishikawa. 2002. Millimeter-wave microstrip array antenna with high efficiency for automotive radar systems. *R&D Review of Toyota CRDL* 37, 2 (2002), 7–12.

[38] A. A. Iskandar, R. Kolla, K. Schilling, and W. Voelker. 2016. A wearable 1-lead necklace ECG for continuous heart rate monitoring. In *2016 IEEE 18th International Conference on e-Health Networking, Applications and Services (Healthcom).* 1–4. https://doi.org/10.1109/HealthCom.2016.7749480

[39] John David Jackson. 2007. *Classical electrodynamics.* John Wiley & Sons.

[40] Vincent Jacquemet. 2015. Modeling left and right atrial contributions to the ECG: a dipole-current source approach. *Computers in biology and medicine* 65 (2015), 192–199.

[41] Delaram Jarchi and Alexander J Casson. 2016. Estimation of heart rate from foot worn photoplethysmography sensors during fast bike exercise. In *2016 38th Annual International Conference of the IEEE Engineering in Medicine and Biology Society (EMBC).* IEEE, 3155–2158.

[42] Poul Jo/rgensen, Jens Oddershede, Preben Albertsen, and Nelson HF Beebe. 1978. Frequency-dependent polarizabilities and Verdet constants for He, Be, CO, and FH. *The Journal of Chemical Physics* 68, 6 (1978), 2533–2543.

[43] Kristian Kroschel and Armin Luik. 2018. Laser-based remote measurement of vital parameters of the heart. In *Optical Sensing and Detection V*, Vol. 10680. International Society for Optics and Photonics, 106800S.

[44] Elina Lampinen, Tino Karolaakso, Anu Karvonen, Jukka Kaartinen, Virpi-Liisa Kykyri, Jaakko Seikkula, and Markku Penttonen. 2018. Electrodermal Activity, Respiratory Sinus Arrhythmia, and Heart Rate Variability in a Relationship Enrichment Program. *Mindfulness* 9, 4 (2018), 1076–1087.

[45] Huining Li, Chenhan Xu, Aditya Singh Rathore, Zhengxiong Li, Hanbin Zhang, Chen Song, Kun Wang, Lu Su, Feng Lin, Kui Ren, et al. 2020. VocalPrint: exploring a resilient and secure voice authentication via mmWave biometric interrogation. In *Proceedings of the 18th Conference on Embedded Networked Sensor Systems.* 312–325.

[46] Feng Lin, Chen Song, Yan Zhuang, Wenyao Xu, Changzhi Li, and Kui Ren. 2017. Cardiac scan: A non-contact and continuous heart-based user authentication system. In *Proceedings of the 23rd Annual International Conference on Mobile Computing and Networking.* 315–328.

[47] Zichao Long, Yiping Lu, Xianzhong Ma, and Bin Dong. 2018. Pde-net: Learning pdes from data. In *International Conference on Machine Learning.* PMLR, 3208–3216.

[48] Jaakko Malmivuo and Robert Plonsey. 1995. *Bioelectromagnetism. 12. Theory of Biomagnetic Measurements.* 227–254.

[49] M Sabarimalai Manikandan and Samarendra Dandapat. 2007. Wavelet energy based diagnostic distortion measure for ECG. *Biomedical Signal Processing and Control* 2, 2 (2007), 80–96.

[50] Mavuto M Mukaka. 2012. A guide to appropriate use of correlation coefficient in medical research. *Malawi medical journal* 24, 3 (2012), 69–71.

[51] Andrea Němcová, Radovan Smíšek, Lucie Maršánová, Lukáš Smital, and Martin Vítek. 2018. A comparative analysis of methods for evaluation of ECG signal quality after compression. *BioMed research international* 2018 (2018).

[52] Ramon Nitzberg. 1972. Constant-false-alarm-rate signal processors for several types of interference. *IEEE Trans. Aerospace Electron. Systems* 1 (1972), 27–34.

[53] RK Orkand and R Niedergerke. 1964. Heart action potential: dependence on external calcium and sodium ions. *Science* 146, 3648 (1964), 1176–1177.

[54] James D Pierce Jr. 2009. *Electromagnetic compatibility (EMC) requirements for military and commercial equipment.* Technical Report. NAVAL POSTGRADUATE SCHOOL MONTEREY CA.

[55] Sebastian Ruder. 2016. An overview of gradient descent optimization algorithms. *arXiv preprint arXiv:1609.04747* (2016).

[56] Clayton Scott and Robert Nowak. 2005. A Neyman-Pearson approach to statistical learning. *IEEE Transactions on Information Theory* 51, 11 (2005), 3806–3819.

[57] Michael Scriven. 1975. *Evaluation bias and its control.* Citeseer.

[58] Shimmer Sensing. 2021. Consensys ECG. https://www.shimmersensing.com/products/ecg-development-kit

[59] Granville Sewell. 2012. *Analysis of a finite element method: PDE/PROTRAN.* Springer Science & Business Media.

[60] Fred Shaffer and JP Ginsberg. 2017. An overview of heart rate variability metrics and norms. *Frontiers in public health* 5 (2017), 258.

[61] Wenzhe Shi, Jose Caballero, Lucas Theis, Ferenc Huszar, Andrew Aitken, Christian Ledig, and Zehan Wang. 2016. Is the deconvolution layer the same as a convolutional layer? *arXiv preprint arXiv:1609.07009* (2016).

[62] Jorge Sola and Joaquin Sevilla. 1997. Importance of input data normalization for the application of neural networks to complex industrial problems. *IEEE Transactions on nuclear science* 44, 3 (1997), 1464–1468.

[63] Kasper Sørensen, Samuel E Schmidt, Ask S Jensen, Peter Søgaard, and Johannes J Struijk. 2018. Definition of fiducial points in the normal seismocardiogram. *Scientific reports* 8, 1 (2018), 1–11.

[64] Yu Sun and Nitish Thakor. 2015. Photoplethysmography revisited: from contact to noncontact, from point to imaging. *IEEE Transactions on Biomedical Engineering* 63, 3 (2015), 463–477.

[65] Garima Chandra Tanvi Sapatnekar. 2017. Electrocardiograph (ECG) Market Size, Share, and Forecast. https://www.alliedmarketresearch.com/electrocardiograph-ECG-market

[66] Natalia A Trayanova and John Jeremy Rice. 2011. Cardiac electromechanical models: from cell to organ. *Frontiers in physiology* 2 (2011), 43.

[67] Lev A Vainshtein. 1988. Electromagnetic waves. *MIzRS* (1988).

[68] O Rebecca Vincent, Olusegun Folorunso, et al. 2009. A descriptive algorithm for sobel image edge detection. In *Proceedings of Informing Science & IT Education Conference (InSITE)*, Vol. 40. Informing Science Institute California, 97–107.

[69] Xuyu Wang, Chao Yang, and Shiwen Mao. 2017. PhaseBeat: Exploiting CSI phase data for vital sign monitoring with commodity WiFi devices. In *2017 IEEE 37th International Conference on Distributed Computing Systems (ICDCS)*. IEEE, 1230–1239.

[70] MR Webb. 1991. A mm-wave four-port quasi-optical circulator. *International journal of infrared and millimeter waves* 12, 1 (1991), 45–63.

[71] David H Wolpert and William G Macready. 1997. No free lunch theorems for optimization. *IEEE transactions on evolutionary computation* 1, 1 (1997), 67–82.

[72] Zhicheng Yang, Parth H Pathak, Yunze Zeng, Xixi Liran, and Prasant Mohapatra. 2016. Monitoring vital signs using millimeter wave. In *Proceedings of the 17th ACM International Symposium on Mobile Ad Hoc Networking and Computing*. 211–220.

[73] Yee Guan Yap and A John Camm. 2003. Drug induced QT prolongation and torsades de pointes. *Heart* 89, 11 (2003), 1363–1372.

[74] Simon H Yueh, Richard West, William J Wilson, Fuk K Li, Eni G Njoku, and Yahya Rahmat-Samii. 2001. Error sources and feasibility for microwave remote sensing of ocean surface salinity. *IEEE Transactions on Geoscience and Remote Sensing* 39, 5 (2001), 1049–1060.

[75] Han Zhang, Ian Goodfellow, Dimitris Metaxas, and Augustus Odena. 2019. Self-Attention Generative Adversarial Networks. In *Proceedings of the 36th International Conference on Machine Learning (Proceedings of Machine Learning Research, Vol. 97)*, Kamalika Chaudhuri and Ruslan Salakhutdinov (Eds.). PMLR, 7354–7363. http://proceedings.mlr.press/v97/zhang19d.html

[76] Qingxue Zhang, Dian Zhou, and Xuan Zeng. 2017. Highly wearable cuff-less blood pressure and heart rate monitoring with single-arm electrocardiogram and photoplethysmogram signals. *Biomedical engineering online* 16, 1 (2017), 23.

[77] Mingmin Zhao, Fadel Adib, and Dina Katabi. 2016. Emotion recognition using wireless signals. In *Proceedings of the 22nd Annual International Conference on Mobile Computing and Networking*. 95–108.

[78] Run Zhao, Dong Wang, Qian Zhang, Haonan Chen, and Anna Huang. 2018. CRH: A Contactless Respiration and Heartbeat Monitoring System with COTS RFID Tags. In *2018 15th Annual IEEE International Conference on Sensing, Communication, and Networking (SECON)*. IEEE, 1–9.

[79] Yaniv Zigel, Amon Cohen, and Amos Katz. 1996. A diagnostic meaningful distortion measure for ECG compression. In *Proceedings of 19th convention of electrical and electronics engineers in Israel*. IEEE, 117–120.

[80] Yaniv Zigel, Arnon Cohen, and Amos Katz. 2000. The weighted diagnostic distortion (WDD) measure for ECG signal compression. *IEEE transactions on biomedical engineering* 47, 11 (2000), 1422–1430.